

Conductance Properties of Carbon-Based Molecular Junctions

Giorgos Fagas^{a*} and Agapi Kambili^b

^a *NMRC, Lee Maltings, Prospect Row, Cork, Ireland*

^b *Institut für Theoretische Physik, Universität Regensburg, 93040 Regensburg, Germany*

(Dated: October 30, 2018)

We present a comprehensive study of the properties of the off-resonant conductance spectrum in oligomer nanojunctions between graphitic electrodes. By employing first-principle-based methods and the Landauer approach of quantum transport, we identify how the electronic structure of the molecular junction components is reflected in electron transport across such systems. For virtually all energies within the conduction gap of the corresponding idealised polymer chain, we show that: a) the inverse decay length of the tunnelling conductance is intrinsically defined by the complex-band structure of the molecular wire despite ultrashort oligomer lengths of few monomer units, and b) the contact conductance crucially depends on both the local density of states on the metal side and the realised interfacial contact.

I. INTRODUCTION

Molecular electronics has been an active research field [1, 2, 3] since the early seventies, when a rectifier based on a single organic molecule was proposed [4]. Extensive experimental [5, 6, 7, 8, 9, 10, 11, 12, 13, 14, 15, 16, 17, 18, 19] and theoretical [20, 21, 22, 23, 24, 25, 26, 27, 28, 29, 30, 31, 32, 33, 34, 35, 36, 37, 38, 39, 40] investigations have examined the electronic response of a single molecule hybridising with metals which act as donor and acceptor reservoirs. Electron transport across metal/molecule/metal junctions (MMMs) depends crucially on the details of the contacts and the exact choice of materials, so that the fundamental mechanisms have been highly controversial. Fine tuning may lead to a range of behaviours in the current-voltage characteristics [2]. Examples include negative differential resistance, strong rectification, molecular memory phenomena, and even the Coulomb blockade effect, a hallmark of mesoscopic physics.

For a class of MMMs increasing consensus based on experimental findings [13, 14, 15, 16, 17, 18, 19] points to a dominant transport mechanism, namely, to through-bond tunnelling. Such setups typically consist of relatively short oligomers like alkane [13, 14, 15, 16] and phenyl-based chains [17, 18, 19] which are covalently bonded either directly or via anchor groups to the metallic electrodes. The metal of choice is usually Au for its noble properties. Most recently, junctions with graphitic and mercury drop contacts have also been investigated [18].

Experimental results show temperature independent electron transport and a conductance g which decreases exponentially versus the molecular length L , with an inverse decay length β deriving from the oligomer. Namely,

$$g(E_F, V) = g_o(E_F, V)e^{-\beta(E_F, V)L}, \quad (1)$$

where E_F denotes the equilibrium Fermi energy. The pre-exponential factor g_o is determined by the actual interfacial contact. In most realisations, measured quantities do not depend on the source-drain voltage V for low bias. In another experiment [15], a weak dependence has been indicated. Nevertheless, such behaviour is consistent with the picture of coherent off-resonant tunnelling across the molecular bridge.

Eq. 1 has been theoretically investigated deep inside the tunnelling regime, both analytically for π -electron models of increasing complexity [41, 42, 43] and numerically for some realistic MMMs [29, 44, 45]. In those studies, electron-vibrational coupling has been disregarded and the zero temperature T , zero bias limit have been taken. Up to T not much lower than room temperature ($\leq 25\text{meV}$), all assumptions constitute a reasonable approximation for specific molecular junctions. This depends on the molecular vibrational frequencies and conformational barriers, electron resident times, and the non-equilibrium electrostatic potential profile. Moreover, these assumptions are in agreement with the above experiments, allowing for an electrical response that is predominantly a property of equilibrium conditions, such as the band line-up or charge relaxation [20, 21, 22, 23, 24, 25, 26], the optimised atomic configuration of the molecular bridge [27, 28, 29, 30], and the contact microstructure [31, 32, 33, 34, 35, 36, 37, 38, 39, 40].

Electron transport across a molecular junction has a lot in common with the intramolecular or donor-bridge-acceptor (DA) electron transfer. The exponential dependence of the conductance in Eq. 1 is reminiscent of the well-studied McConnell's superexchange mechanism in the weak coupling limit [46, 47, 48], where

$$k_{DA} = \frac{2\pi}{\hbar} |H_{DA}|^2 F \sim e^{-\beta(E)L}. \quad (2)$$

A connection between the electron transfer rate k_{DA} and the conductance has been given by Nitzan [49] in certain limits. H_{DA} is the coupling between donor and acceptor electronic states at a potential surface crossing energy E , and F is the Franck-Condon factor. However, the continuum of states of the reservoirs and their constraints

*gfagas@nmrc.ie

redefine the problem and have to be explicitly considered for a full account of the conduction properties. From this viewpoint, a transport calculation across the whole system is required.

Mujica *et al* [41] generalised previous analytical results of Everson and Karplus [47] on electron transfer across a single-orbital tight-binding linear homogeneous chain, to study conductance properties. Their studies revealed the exponential length decrease for energies far-off the energy spectrum of the molecular bridge. Onipko *et al* [42] found an approximate solution for conjugated oligomers in the π -electron model. By disregarding the effect of the electrodes to the molecular electronic structure in the tunnel limit $\beta(E)L \gg 1$, their results closely resemble the electron transfer problem. However, they provide a simple expression for g_o . Using extended Hückel calculations, Joachim with Vinuesa [44] and Magoga [45] have studied numerically the conductance at E_F of several relatively long conjugated molecules, where E_F falls in the middle of the wire conduction gap. They established that the damping factor is a characteristic property of the wire and that g_o is related to the contact realisation of the bridge, in agreement with Onipko *et al* [42]. Moreover, an analytic expression for β was derived within a simple model [43] and its properties were studied within a level-repulsion approach of Random Matrix Theory [50, 51].

Most recently, Joachim and Magoga [52], and Tomfohr and Sankey [53], provided independently approximate expressions for the effective mass of electrons in MMMs tunnelling through the oligomer-induced barrier. They considered the ideal polymer limit and approximated β to the spatial decay parameter of the wavefunction. This possibility has been conjectured in many of the aforementioned studies. Tomfohr and Sankey studied the local DOS decay parameter of octanedithiols between Au (111) surfaces and found good qualitative agreement with the imaginary part of the wavevector of wavefunctions in the forbidden energy domain of the corresponding one-dimensional crystal, namely, the complex-band structure [54, 55].

In this paper, we examine off-resonant electron transport across molecular junctions in view of the new experiments and advances of theoretical concepts. In particular, we provide a comprehensive analysis of the entire conductance spectrum inside the Highest-Occupied-Molecular-Orbital–Lowest-Unoccupied-Molecular-Orbital (HOMO-LUMO) gap E_g^M of phenyl-based oligomers, as a function of the number of monomer units. We focus on studies of oligo-phenyl-ethynyl (OPE), planar and non-planar oligo-para-phenyl (OPP) molecular wires covalently bonded to electrodes consisting of graphitic ribbons. First-principle-based methods are employed to calculate the electronic structure of the molecular junction components, and the conductance in the Landauer approach of quantum transport.

We find that the conductance is almost always an exponentially decreasing function of length and *not only*

for $\beta(E)L \gg 1$. We observe tunnelling characteristics for ultrashort oligomer molecular junctions and/or energies not far-off the edges of the conduction gap E_g of the corresponding polymer (PPE and PPP, respectively). The contact conductance can be approximately written as $g_o(E) = \Gamma_L^2 \Gamma_U^2 f(E)$, where $\Gamma_{L/U}$ describes the atomic coupling at the molecule/metal interface, and $f(E)$ reflects both the electrode and molecular spectral properties. The inverse decay length is determined by the energy spectrum of the polymer when extended to include complex wavevectors. A remarkable one-to-one correspondence to the imaginary part of the latter is found for all cases. A brief account of the complex wavevector mapping applied to PPE has been previously given by the authors [58]. Mathematically, the problem of scattering through finite periodic systems has been studied to some extent in Ref. [59].

Since interfacial barriers in our systems are generally lower than the ones realised in the experiments, these results explain qualitatively the observations in molecular junctions of a handful of monomers. In addition, they acquire special importance when recognising that E_F may lie anywhere inside the gap. It is in fact common knowledge that it is difficult to *a priori* locate E_F which crucially depends on the combination of anchor groups and electrodes.

The choice of OPP and OPE as molecular bridges in our MMMs is dictated by the usual experimental setups. Graphene-like macromolecules have been synthesised [60] and studied theoretically [39] as the active components of molecular junctions. Moreover, driven by a vision of purely carbon electronics experiments with pyrolytic graphite as one of the metals have been reported [18], for which the structures we study constitute a first approximation. On the other hand, the graphitic ribbons we consider have some special electronic states [61, 62, 63, 64, 65] with large local density of states around E_F , which are responsible for additional features in the conductance. In analogy to other carbon-based systems [36] in which they give much richer spectra, these states provide an extra channel for resonant transport within the HOMO-LUMO gap of the molecular bridge [66]. As a function of the length of oligomers, they also compete against the exponential law Eq. 1.

The structure of the paper is as follows. In Sec. II we briefly introduce the theoretical methods that we used, and the details of the investigated systems. In Sec. III we present the electronic structure of the studied molecular junctions with emphasis on the properties relevant to the aimed transport. We also analyse the concept of complex-band structure. The conductance properties are discussed in Sec. IV. Finally, we make some concluding remarks.

II. COMPUTATIONAL FRAMEWORK

A. Electronic Structure and Transport Properties

The electronic structure of the oligomer as well as that of the electrodes is treated within an approach based on Density Functional Theory (DFT) in the local density approximation (LDA). By employing a linear combination of atomic orbitals, the method falls into the class of tight-binding (TB)-DFT. It has been successfully applied to the calculation of properties of a range of materials including semiconductors, carbon nanotubes, fullerenes, DNA and proteins [36, 67, 68, 69, 70].

The single-particle electronic Kohn-Sham eigenstates ψ_i of the system are expanded in a non-orthogonal basis set $\varphi_\mu(\mathbf{r} - \mathbf{R}_\mu)$ taken as a valence basis localised at the ionic positions \mathbf{R}_μ , namely

$$\psi_i(\mathbf{r}) = \sum_{\mu} c_{\mu}^i \varphi_{\mu}(\mathbf{r} - \mathbf{R}_{\mu}). \quad (3)$$

When this *Ansatz* is substituted in the Kohn-Sham equations for ψ_i , it yields a set of algebraic equations

$$\sum_{\nu} (H_{\mu\nu}^{TB} - S_{\mu\nu}^{TB} E_i) c_{\nu}^i = 0. \quad (4)$$

The crucial step in deriving Eq. 4 is a further approximation of the full many-body problem by a tight-binding Hamiltonian which is a function of atomic densities [68]. The *a priori* parametrisation scheme for the two-centre, distance dependent Hamiltonian, $H_{\mu\nu}^{TB}$, and overlap, $S_{\mu\nu}^{TB}$, matrix elements provides an efficient algorithm for electronic structure calculations. Explicit computational details are given in Ref. [67]. Even though the form of Eq. 4 is evidently that of the extended Hückel, all necessary matrix elements are determined without introducing empirical parameters.

To calculate the conductance, we adopt the Landauer picture of quantum transport [56, 57] in combination with the TB-DFT. In this formalism, the current through a structure is expressed in terms of the transmission function $\bar{T}(E, V)$. The latter denotes the probability of electrons with energy E to propagate coherently across the system between the two electron reservoirs. Reading explicitly,

$$I = \frac{2e}{h} \int_{-\infty}^{+\infty} dE \bar{T}(E, V) [f(E - \mu_1, T) - f(E - \mu_2, T)], \quad (5)$$

where $f(E - \mu, T)$ is the Fermi function, and $\mu_{1,2}$ refer to the chemical potentials of the two electrodes (1,2). The factor 2 in the equality implies spin degeneracy.

Here, we take the low bias limit and drop the voltage dependence of \bar{T} , which in general is a function of the exact electrostatic profile. This approximation yields accurate results for $V \sim 0.1\text{eV}$ [24]. It is also expected to hold

for a wider bias range for voltages dropping mostly at the contacts. Finally, the transmission function is given by the Green's function method of quantum transport via

$$\bar{T}(E_F) = Tr \left[\mathbf{\Gamma}_1 \mathbf{G}_M^r \mathbf{\Gamma}_2 \mathbf{G}_M^{r\dagger} \right], \quad (6)$$

where $\mathbf{G}_M^r(E) = (E\mathbf{S}_M^{TB} - \mathbf{H}_M^{TB} - \mathbf{\Sigma})^{-1}$ is the retarded molecular Green function at equilibrium.

Using the Löwdin projection technique, \mathbf{G}_M^r is dressed by a self-energy interaction $\mathbf{\Sigma} = \mathbf{\Sigma}_1 + \mathbf{\Sigma}_2$ that takes into account the hybridisation of the molecular bridge with the metals. The spectral widths $\mathbf{\Gamma}_{1,2}$ act as an effective coupling to the electronic states of the electrodes. $\mathbf{\Sigma}_{1,2}$ and $\mathbf{\Gamma}_{1,2}$ are given by

$$\mathbf{\Sigma}_{1,2}(E) = \mathbf{J}_{1,2-M}^{\dagger}(E) \mathbf{G}_{1,2}^r(E) \mathbf{J}_{1,2-M}(E) \quad (7)$$

and

$$\mathbf{\Gamma}_{1,2}(E) = i \left[\mathbf{\Sigma}_{1,2}(E) - \mathbf{\Sigma}_{1,2}^{\dagger}(E) \right], \quad (8)$$

respectively. $\mathbf{J}_{1,2-M} = E\mathbf{S}_{1,2-M} - \mathbf{H}_{1,2-M}^{TB}$ is the generalised expression for a non-orthogonal basis, instead of the simple occurrence of the coupling matrix $\mathbf{H}_{1,2-M}^{TB}$ between the electrodes and the molecule. The retarded Green function $\mathbf{G}_{1,2}^r$ of the leads is calculated by the Sanvito *et al* algorithm [71], also extended to include the overlap between atomic orbitals. The above procedure mainly involves the manipulation of $N_M \times N_M$ matrices, where N_M is the number of atomic orbitals taken at positions on the molecule. Exception is Eq. 7 that includes electrode degrees of freedom. However, interactions are of short-range due to the tight-binding approximation, and matrix dimensions never exceed $\sim N_M$.

In what follows, we focus on generic properties of electron transport across carbon-based molecular junctions. To this end, we study the conductance spectrum which is defined via

$$g(E) = \frac{2e^2}{h} \bar{T}(E). \quad (9)$$

It follows from Eq. 5 within the linear response that the above expression at E_F strictly coincides with the conductance for very low bias. For finite but small voltages such that non-equilibrium effects are insignificant generalised formulae involving $g(E)$ may be derived (cf [6]). However, a complete investigation of the voltage dependence is out of the scope of the paper and is left for the future. We note the main effect of moderate-to-room temperature is to broaden features of the conductance at the $\sim 0.1\text{eV}$ scale.

B. System Specifics

We consider all-carbon molecular junctions such as those depicted in Fig. 1. The electrodes are (zigzag)

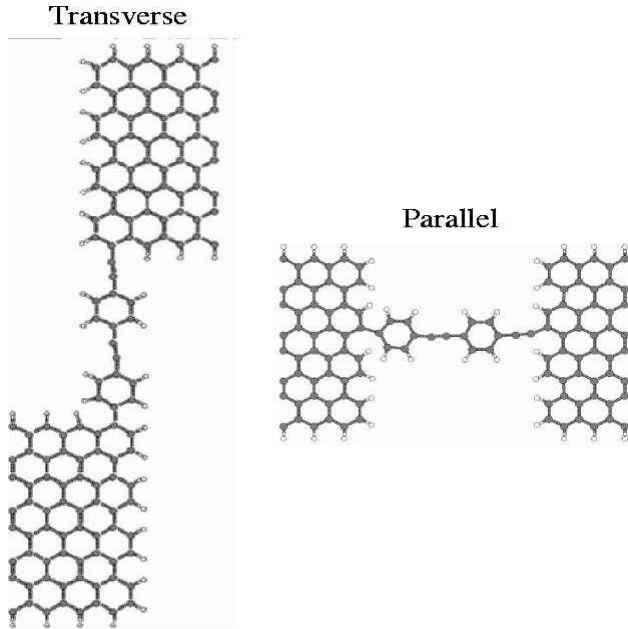


FIG. 1: A representative molecular junction among those studied is the structure of diphenyl-ethynylene ($N = 2$) bonded to two graphitic electrodes along either the zigzag (left) or the armchair (right) edge. Open circles denote hydrogen atoms. See Sec. IIB for more details.

graphitic ribbons of the indicated width and infinite extension along the carbon boundary of zigzag shape. By taking into account the weak inter-plane interactions in graphite, we isolate a single plane for simplicity. The molecule is a conjugated molecular wire of a few repeated monomer units, N , also taken as our length unit. To demonstrate topological effects on the conductance, we initially examine two different types of junctions; one with the oligomer being attached to the electrodes along the zigzag edge ('transverse' configuration), and one with the wire connected to the armchair side of the ribbons ('parallel' configuration), as shown in Fig. 1. All dangling bonds at edge sites are saturated by hydrogen atoms (open circles in Fig. 1), so that they do not contribute to the density of states around the Fermi energy E_F .

The molecular bridges under investigation are formed by two chemically different oligomers, and conformationally varying: a) oligo-phenyl-ethynylene, and b) planar and non-planar oligo-para-phenylene which differs from OPE in that it does not have the triple carbon-carbon bond between the benzene rings. This makes OPP more flexible with energetically favourable conformation the non-planar one. Tetrahedral angles between benzene rings may vary from 45° for very small oligomers to 27° for polymers [73, 74]. At room temperature, ring rotational motion occurs between the planar and non-planar conformation. When the temperature is cooled down both possibilities may be realised in experiments with self-assembled monolayers [18]. Therefore, we consider several geometries as summarised in Fig. 2.

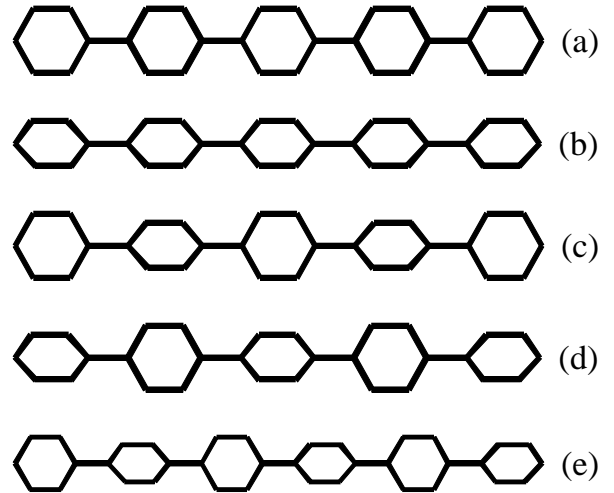


FIG. 2: Configurations of oligo-para-phenyl molecular bridges studied in this paper. They are distinguished between odd and even N , e.g. for (a)-(d), $N = 5$, and for (e), $N = 6$, respectively. The graphene ribbon electrodes contacted at the end-sites on both sides are in-plane with the page. The tetrahedral angle for non-planar OPP ((c)-(e)) and the contact geometry (b) is 45° .

The structures (molecular bridge+electrodes) are optimised in all calculations. To simulate the bulk electrodes, a constrained atomic optimisation of junctions such as those of Fig. 1 is performed. Graphene atoms away from the oligomer/ribbon interfacial bond by approximately $3 \times$ hexagonal lattice constant remain immovable in the positions they assume in perfect graphene. The inner carbon atoms, which look unsaturated in Fig. 1, are bonded to H to avoid spurious effects during optimisation. As input, initial single C-C bond lengths equal 1.39\AA , triple C-C bond lengths equal 1.2\AA , and C-H distances equal to 1.09\AA . All angles are at 120° .

III. ELECTRONIC STRUCTURE

A. Electrodes: Graphene Ribbons

There has been an extensive interest in the properties of nano-graphitic materials recently. Specifically, ribbon-shaped graphite as in Fig. 1 is intensively investigated and the scope of this section is limited to pointing out the electronic properties that are crucial for the conductance of the systems we study. These are related to peaks in the density of states (DOS). Such features arise from the low dimensionality of the ribbons, the topology of their edges, and the hexagonal lattice.

In Fig. 3(a) we plot the density of states of a ribbon with width $M = 4$. The latter is given by the maximum number of honeycomb cells that can be found in a cross-section. The ribbon DOS is contrasted with the DOS of bulk graphene (dotted line). It exhibits the characteristic van-Hove singularities of quasi-one-dimensional

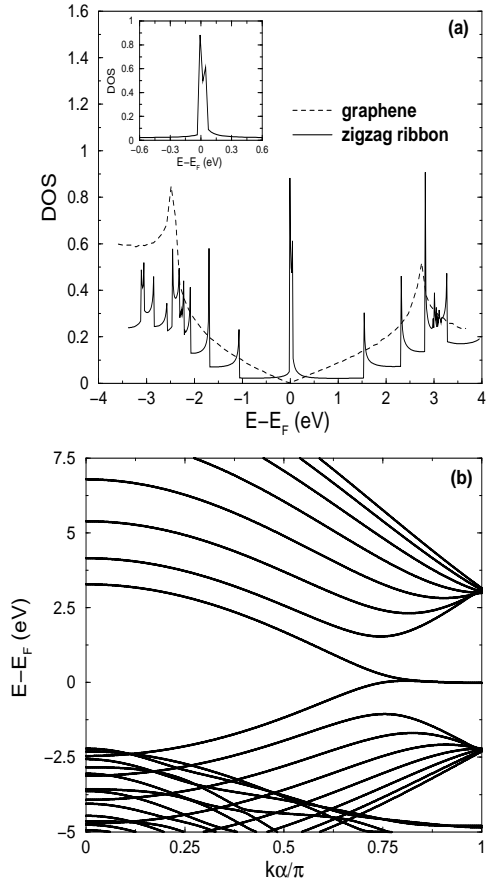


FIG. 3: (a) Density of states (DOS) for graphitic systems; dashed and solid lines correspond to graphene and a zigzag ribbon, respectively. The inset shows the DOS of the ribbon at energies around E_F . (b) Band structure of a zigzag ribbon of width $M = 4$.

systems. Apart from that one around E_F , which we discuss separately, their peak positions depend on the width, and they are present independent of the topology of the edges.

The double peak of the ribbon DOS around E_F (inset of Fig. 1) is generic to graphene edges with a zigzag geometry [61, 62]. For zigzag ribbons, which are periodically repeated structures, this develops from two partially flat bands at the Fermi level, conferring metallic properties [65]. To rationalise the above features, the band structure is shown in Fig. 3(b), which is in good agreement with less approximate plane-wave DFT calculations [63, 64].

The electronic states corresponding to the low energy bands are termed edge states. This reflects the property of wavefunction localisation near the edges. In fact, in a seminal paper of Lee and Joannopoulos [72] on the calculation of surface states, the honeycomb lattice with zigzag edges was presented as a paradigm. Other specific studies on tight-binding models [61, 63, 65] of graphene revealed a single peak arising at E_F , which owes to the

simplicity of the π -electron Hamiltonian. In those, the topological origin of the peak and its stability against disorder were also established.

Finally, we note that for applications in molecular electronics, one should, more precisely, look at the local DOS since the local electronic structure is most important. The overall DOS may be misleading. For example, electronic states in a quasi-one-dimensional square lattice or simply those of the Anderson-Newns model of chemisorption possess van-Hove singularities but exhibit a smooth local DOS. This owes to a cancellation of border zone anomalies (group velocity $v_g \propto \sin(k\alpha)$) by the longitudinal component of the wavefunction [34]. Nevertheless, this does not apply to our discussion. Using the analogy of graphene ribbons to carbon nanotubes, and in agreement with the topological arguments, we employ a previous result [34] stating that for states with zero group velocity outside the border zone, as in Fig. 3, no such cancellation occurs. Indeed, we have calculated the local density of states at the carbon atoms on the electrode sides which are bonded to the oligomers for all studied molecular junctions. Unless stated, we have found small deviations from the DOS of Fig. 3 (see also inset of Fig. 5), mainly caused by the oligomer chemisorption.

B. Molecular Wires: Poly-Phenyl-Ethynylene (PPE) and Poly-Para-Phenylene (PPP)

A core result of this paper relates to the fingerprints of the electronic band structure of the perfect one-dimensional crystals that correspond to the molecular bridges of Fig. 1 and 2, namely, PPE and PPP, respectively. In particular, since we study off-resonant electron transport within the HOMO-LUMO gap, we are not interested in the usual band structure defined for real Bloch vectors k . As explained below, we need instead to quantify the spatial decay of electronic evanescent states for energies within the energy gap E_g between the top of the valence, E_v , and the bottom of the conduction, E_c , bands. The latter develop from the HOMO and LUMO, respectively, of long wires.

When molecular junctions are formed the molecular electronic states hybridise with the metal wavefunctions giving a finite width in energy space and a renormalised HOMO-LUMO gap $E_g^M (\geq E_g)$. For energies within the gap, matching to the metal side implies decaying wavefunctions within the molecule. These states are the analogue of the metal-induced gap states (MIGS) in metal-insulator (or metal-semiconductor) junctions [55]. MIGS are responsible for the overall finite DOS within the E_g^M for short molecular wires because of contributions coming from both electrodes [20]. For longer wires, the MIGS are mainly located near the interfaces on either side of the molecule. Indeed, by looking at the positional dependence of the local DOS, such behaviour has been observed for Si nanowires between Al electrodes [75] and alkanethiol chains between Au (111) surfaces [53, 76].

We come back to these points in Sec. IV B.

By assuming that interfacial effects at a molecular junction are not dominant, we turn our attention to decaying states in the idealised underlying periodic systems of PPE and PPP. In this case, it is well known that wavefunctions vanish exponentially in space in the forbidden energy domain. The decay parameter is quantified by the imaginary component of Bloch vectors ($k \equiv q - i\kappa$). The latter are obtained via the method of the complex-band structure, which may be understood as an extension of the conventional band structure to the complex plane [54, 55]. Computational schemes are intimately related to the quest for surface states [72] and the method is as follows.

In all cases, one has to solve the Schrödinger equation in a periodic potential, which in our tight-binding approximation reads

$$\begin{aligned} & (\mathbf{H}_{m,m}^{TB} + \mathbf{H}_{m,m+1}^{TB} e^{ika} + \mathbf{H}_{m-1,m}^{TB} e^{-ika}) \phi_k = \\ E_k & (\mathbf{S}_{m,m}^{TB} + \mathbf{S}_{m,m+1}^{TB} e^{ika} + \mathbf{S}_{m-1,m}^{TB} e^{-ika}) \phi_k. \end{aligned} \quad (10)$$

Here, the matrices $\mathbf{H}_{i,j}^{TB}$ and $\mathbf{S}_{i,j}^{TB}$ are defined as containing the Hamiltonian and overlap matrix elements, respectively, between the i th and j th unit cells. a is the lattice constant.

To obtain the complex-band structure, one follows the opposite procedure of typical band structure calculations in which the solution of the eigenvalue problem of the Hamiltonian yields the energy spectrum for any real k . The spectrum of k vectors associated with any real energy E is sought. Therefore, it is useful to transform Eq. 10 from an eigenvalue problem for E_k to an eigenvalue problem for $\lambda \equiv e^{ika}$. This problem resembles finding the eigenvalues of the transfer matrix. It may be cast in a generalised eigenvalue problem via

$$\begin{pmatrix} \mathbf{H}_{m,m} - E\mathbf{S}_{m,m} & \mathbf{H}_{m-1,m} - E\mathbf{S}_{m-1,m} \\ \mathbf{I} & \mathbf{0} \end{pmatrix} \tilde{\phi}_\lambda = \lambda \begin{pmatrix} -(\mathbf{H}_{m,m+1} - E\mathbf{S}_{m,m+1}) & \mathbf{0} \\ \mathbf{0} & \mathbf{I} \end{pmatrix} \tilde{\phi}_\lambda, \quad (11)$$

which in contrast to usual formulations, can be used even for singular $\mathbf{H}_{i,j} - E\mathbf{S}_{i,j}$, as it often happens when a localised basis set is employed. When $|\lambda| = 1$, k is real; otherwise k is complex and we have exponentially decaying or growing solutions, which come in conjugate pairs.

The complete band structures of perfect PPE, planar PPP, and non-planar PPP are calculated using Eq. 10 and Eq. 11, and they are shown in Fig. 4(a), 4(b), and 4(c), respectively. At the right panel we present the conventional band structure. The spectrum of the imaginary part of the complex k solutions (negative branch) is plotted at the left panel. Our calculated band structures compare well with those reported for either minimal [30, 53] or plane wave [53, 64] basis sets within other DFT methods in the LDA, both in the real axis and in the complex plane. As expected from studies of the analytic properties of the energy spectrum in the complex

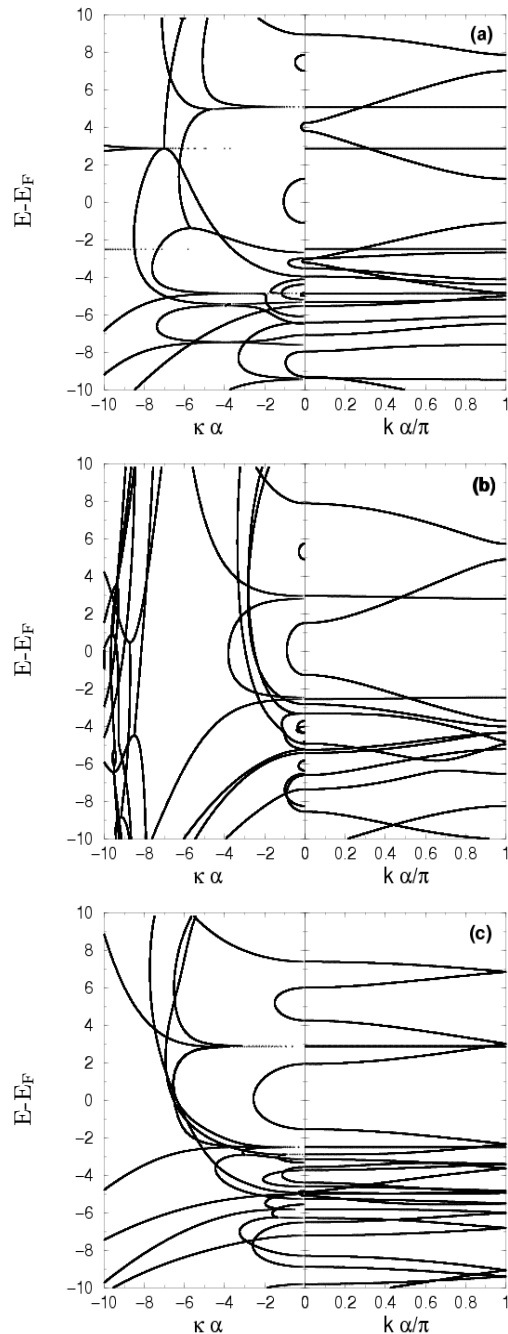


FIG. 4: Electronic band structure for (a) PPE, (b) planar PPP, and (c) non-planar PPP (tetrahedral angle at 45°). The right panel indicates the band structure for real k in the first Brillouin zone, and the left panel the complex-band structure.

plane, the complex-band structure exhibits the connection of real bands between local extrema. Of particular importance for the off-resonant electron transport phenomena we discuss in the next section, is the, so-called, real line which joins the edges of the valence and conduction bands which develop around E_F . It evidently corresponds to the smallest decay of wavefunctions into the molecular region since $|\kappa|$ is minimum, and it is ex-

pected to dominate in tunnelling processes within E_g .

IV. CONDUCTANCE PROPERTIES

A. General Features

The local microstructure of the molecule/electrode interfacial contact, especially for low-dimensional electrodes [33, 34], has been shown to crucially determine the conductance properties of a molecular junction. This is also seen in the transport properties of structures such as those of Fig. 1. To demonstrate the bare effect, we take the parallel and transverse geometries of a diphenylethynyl bridge. As shown in Fig. 5, a clear distinction of the conductance spectrum is evident. Compared to previous studies [32, 36, 37], a remarkable fact is that despite the carbon-carbon covalent bond at the interfaces and the close conformational similarity, there is a prominent dissimilarity in the conductance. The latter can be traced to distinct features in the local DOS for the zigzag and the armchair edge topologies (inset of Fig. 5). An analogue of this effect arising from the molecular bridge contributions to the electronic states at E_F was observed in Refs. [39, 40].

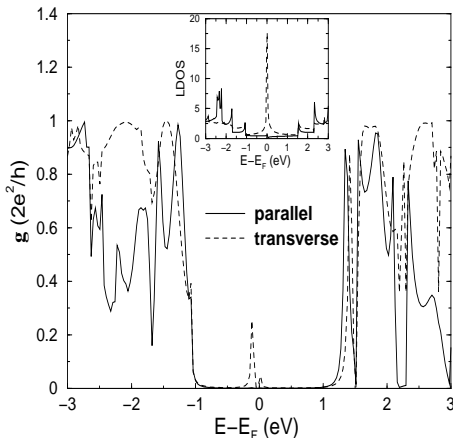


FIG. 5: Conductance spectrum for an OPE wire with length $N = 2$. The solid line corresponds to parallel connection, and the dashed line corresponds to transverse connection (see Fig. 1). The inset shows the local DOS at the two carbon apex-sites for parallel (solid line) and transverse configuration (dashed line).

In particular, the presence of the zigzag edge state has a profound influence. The conductance through the oligomer is non-negligible within the HOMO-LUMO gap, exhibiting a double resonant peak around E_F . For the parallel structure, on the other hand, the conductance is almost vanishing inside E_g^M . The observed conductance resonances are in accordance with previous results showing that due to a large local DOS on the metal side for energies inside the HOMO-LUMO gap, an additional resonant channel becomes available for through-bond con-

duction [36, 66]. Indeed, the inset of Fig. 5 presents the local DOS at edge carbon-atoms of an isolated semi-infinite zigzag ribbon. The dashed line is the local DOS at a carbon atom (saturated by hydrogen) at the zigzag edge, whereas the solid line is for an atom located at an armchair mid-point of the terminated ribbon. The localised state of zigzag edge sites is featured in their local DOS by the characteristic spike, but is missing for armchair edge sites.

To discuss generic properties of off-resonant electron transport properties within E_g , we focus on junctions of the transverse connection, which exhibit additional conductance resonances within E_g^M due to the topology of the electrode/molecule interface ('worst case scenario'). In Fig. 6 we present the logarithm of the conductance spectrum of such carbon junctions, for various lengths N of the oligomers. Plot (a) corresponds to OPE, with valence and conduction band energies of the corresponding polymer wire $E_v = -1.12\text{eV}$ and $E_c = 1.23\text{eV}$, respectively (see Sec. IIIB and Fig. 4). Plot (b) is for planar OPP, with $E_v = -1.27\text{eV}$ and $E_c = 1.48\text{eV}$, and plot (c) is for non-planar OPP, with $E_v = -1.55\text{eV}$ and $E_c = 1.91\text{eV}$. As it has been expected from the above discussion, the conductance exhibits resonances around E_F , which are relatively high for small N . Even though $g(E)$ decreases as N becomes larger, these peaks pertain for all wire lengths. Different oligomers, thus different electronic configurations of the molecule and different coupling to the electrodes, do not obscure the appearance of these conductance resonances, indicating once again that they arise solely from the topology of the electrode contacting surface.

The existence of both peaks in Fig. 6 can be understood by inspection of Fig. 7. There, $\ln(g)$ of an OPE wire of length $N = 5$ is plotted together with the logarithm of the local DOS at the lower (dotted line) and upper (dashed line) electrode apex atoms in contact with the molecule, as a function of the energy. Each of the local DOS at the two contacts has a double peak inside the gap. The energies at which the two conductance peaks appear correspond to the points on the energy range within the gap for which there is large local DOS. This result can be roughly understood from the π -orbital approximation, in which the transmission is related to the local DOS $\nu_{L/U}$ at the lower/upper atomic contacts through the relation $T(E) \propto \nu_L(E)\nu_U(E)|G_{1N}(E)|^2$, G_{1N} being the propagator between the first and the last sites of the molecule [34, 41, 42].

From Fig. 6 we see that the conductance decreases with the length of the molecule. Examining this length dependence in more detail, $\ln(g)$ is plotted as a function of N for selected energies inside the gap, in Fig. 8. Graph (a) is for OPE, graph (b) is for planar OPP, and graph (c) is for non-planar OPP. The energy values of the curves defined by circle and triangle values reside in the left and right side, respectively, of the edge states spectrum. Plots indicated by the squares correspond to one of the two conductance resonances, and the remaining curves

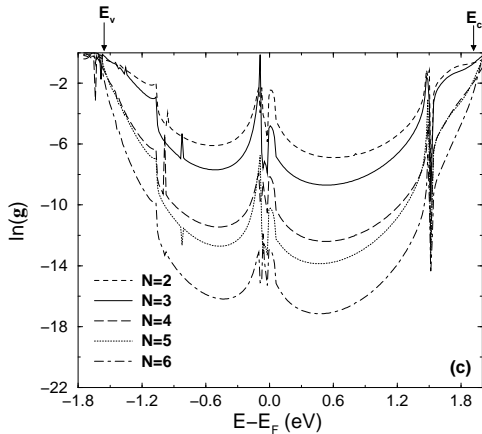
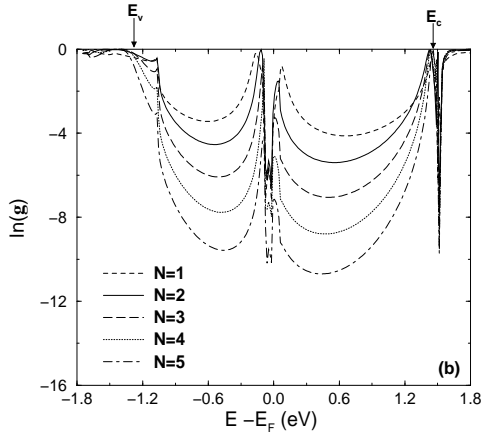
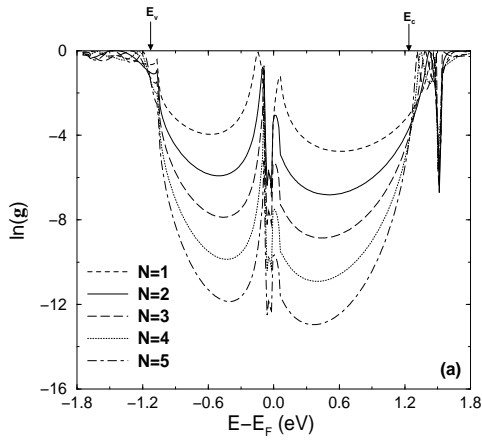


FIG. 6: Logarithm of g versus energy E , for wires of various lengths N . (a) OPE, with valence and conduction band energies $E_v = -1.12\text{eV}$ and $E_c = 1.23\text{eV}$, respectively. (b) planar OPP, with $E_v = -1.27\text{eV}$ and $E_c = 1.48\text{eV}$. (c) non-planar OPP, with $E_v = -1.55\text{eV}$ and $E_c = 1.91\text{eV}$.

(circles) are for an energy between the two peaks. In all three graphs, we evidence three types of curve.

In Figs. 8(a) and 8(b) and for energies away from those of the edge states, $\ln(g)$ falls linearly with N . This is reminiscent of the tunnelling behaviour, Eq. 1. In contrast, for energies at the vicinity of the edge state resonances, an anomalous length dependence appears for

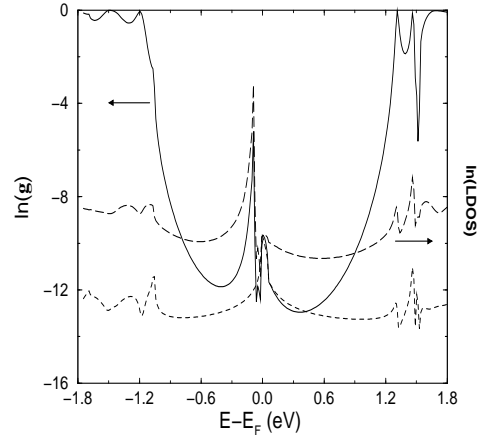


FIG. 7: The left y -axis corresponds to $\ln(g)$, and the right y -axis to the logarithm of the local DOS at the carbon atomic contacts, versus E , for OPE with $N = 5$. The dotted line is the DOS at the contact point between the lower electrode and OPE, and the dashed line is for the DOS at the upper one (see Fig. 1).

very small $N \leq 3$, but as N increases, a linear decrease is also attained. We attribute the former to slight positional shifts of the resonant energies which are evident in the plots as N varies from 1 to approximately 3. After a complete analysis of the conductance spectrum within E_g , we conclude that the exponential law of Eq. 1 holds generally for the entire energy range within E_g and for ultrashort molecular junctions. The observed few deviations are specific to the appearance of "unconventional" resonant channels induced by the electrodes.

For the non-planar OPP (Fig. 8(c)), it appears that $\ln(g)$ decreases with N in an oscillating rather than a linear fashion. A closer look, however, reveals that one should distinguish between the conductance for even and odd N . We should bear in mind the difference in the interfacial contact geometry of the last benzene ring of the oligomer. For odd N , the benzene ring is at the same plane with that of the ribbon, whereas for even N it is positioned at an angle θ away from the plane. This distinction results in different coupling with the electrode, and therefore, in a different contact conductance as we analyse in Sec. IV B. A clear difference is also reflected in the structure of the conductance spectrum around E_F in Fig. 8(c). It follows, however, that the exponential law applies for the two cases separately, with the same inverse decay length. Another viewpoint would be to consider an increase of the molecular length to be given in units of the unit cell of the non-planar PPP.

B. Inverse Decay Length

In the previous Section we established Eq. 1 for virtually all molecular lengths and for any energy in the regime of interest. Here, we identify the damping factor of the

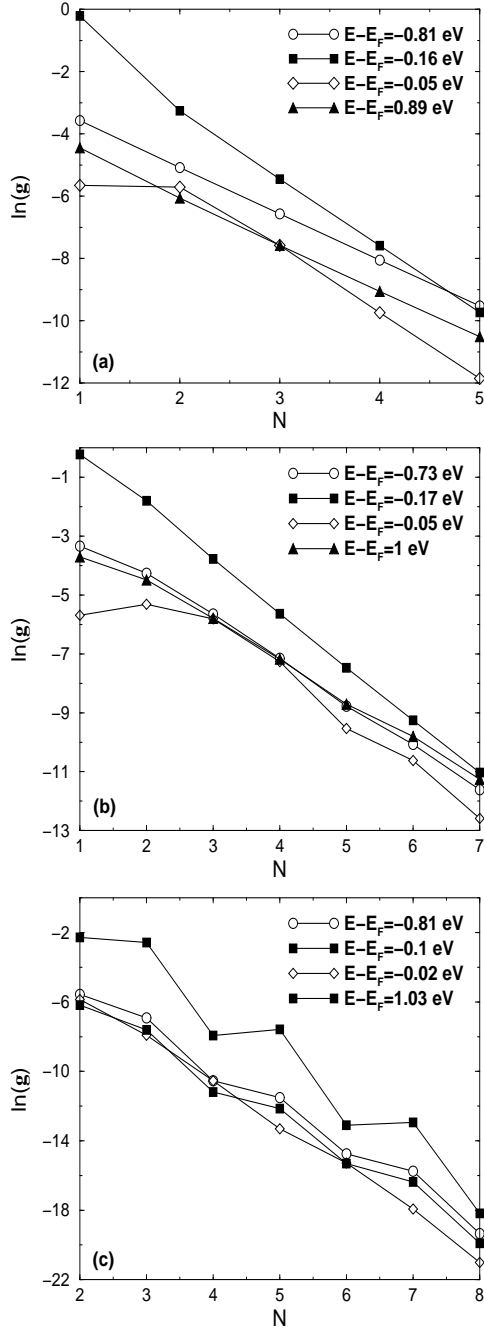


FIG. 8: $\ln(g)$ versus N for various energies within the HOMO-LUMO gap. (a) OPE, (b) planar OPP, and (c) non-planar OPP.

tunnelling conductance of an oligomer junction with the complex-band structure of the corresponding idealised polymer wire discussed in Sec. III B. Consistent with the assumption that, to a first approximation, evanescent states in the junction would coincide with those of the idealised long wire and that those with the smallest $|\kappa|$ are dominating the tunnelling process, in Fig. 9 we isolate the positive branch of the real line $E_c - E_v$ (solid line). The latter equals minus the negative branch. To-

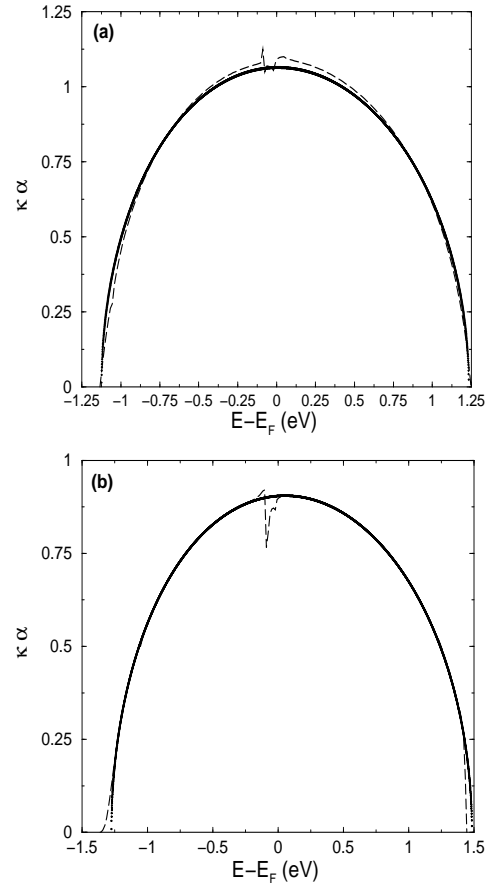


FIG. 9: Complex-band structure ($E_c - E_v$ real line) plotted with a solid curve and tunnelling inverse decay lengths for (a) PPP and OPE, (b) planar PPP and OPP, respectively.

gether we plot the inverse decay length β divided by a factor two (dashed line), which accounts for transport coefficients relating to probability amplitudes rather than wavefunctions. β is numerically obtained from a least-squares fit for the determination of the slope of the lines of Fig. 8. Graph (a) corresponds to OPE and graph (b) to planar OPP. For energies at which the conductance shows anomalous length dependence, we use only data for $N > 2$. In both graphs (a) and (b), there is a remarkable agreement for the entire energy window. There are no deviations from the relation $\beta = 2|\kappa(E)|$ apart from energies at which the graphitic ribbons exhibit a large local DOS.

In the discussion of Fig. 8, we mentioned that for non-planar OPP wires the parity of the length is an important element for the exact conductance spectrum, but that the inverse decay lengths apparently coincide for even and odd N . This is evident in Fig. 8 where the damping factor divided by two is plotted for both cases and is compared to the complex-band structure with the smallest $|\kappa(E)|$. The damping factors for wires with odd (dashed line) and even N (dotted line) are almost identical to each other. Furthermore, they fall on top of the posi-

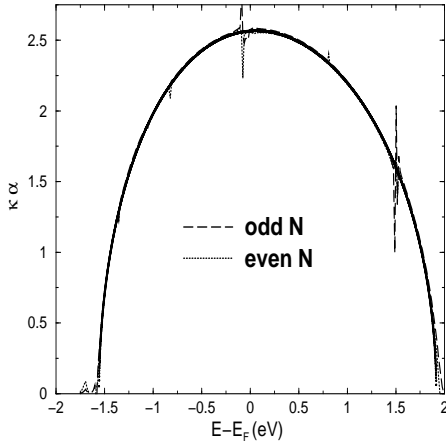


FIG. 10: Complex-band structure ($E_c - E_v$ real line) plotted with a solid curve and tunnelling inverse decay lengths for non-planar PPP and OPP, respectively. The dashed line corresponds to $\beta/2$ from OPP with odd N and the dotted one is for OPP with even N .

tive branch of κ which derives from the conduction and valence bands of non-planar PPP. Once again there is absolute quantitative agreement apart from energy points around singularities in the local DOS (see Fig. 3). It is worth mentioning that all results for the extracted tunnelling decay lengths in oligomer junctions are obtained for the optimised geometries, whereas, the complex-band structure is that of an ideal polymer wire. This shows the robustness of the mapping to small perturbations on atomic positions.

According to the arguments of Sec.III B on the wavefunction matching between the metal and the molecular wire, the density of states inside the molecule should also reflect properties of decaying states. Namely, its projection to an exponential should be possible, at least away from the electrode/wire interface. We examined this approach by calculating the projected density of states within a unit cell (MDOS) of a planar OPP wire of fixed length. In Fig. 11(a), we plot its logarithm as a function of the monomer units i which make up $N = 9$, for energies chosen inside the gap. We see that the logarithm of MDOS falls off almost linearly with i until roughly half of the molecular length is reached, and then $\ln(\text{MDOS})$ increases, again in a linear fashion. Loosely speaking, the decreasing part of each curve corresponds to the decaying metal-induced gap state from the lower electrode whereas the increasing part comes from the gap state of the upper electrode. This holds for relatively long wires as the one presented. For shorter molecular bridges, none of the contributions from each side is dominant. No apparent linearity as in Fig. 11(a) is observed.

To make this analysis quantitative, we calculate a damping factor β_{MDOS} for the density of states, presented in Fig. 11(b). The solid line is again the smallest $|\kappa|$ from the complex band structure of planar PPP (Fig. 9(b)). The dashed and dotted lines represent $\beta_{\text{MDOS}}/2$ from a

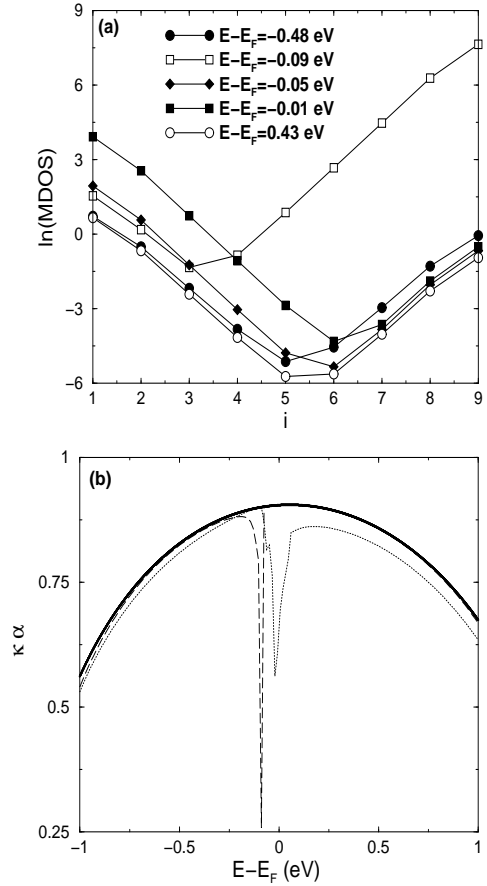


FIG. 11: (a) Logarithm of DOS on a planar OPP wire of length $N = 9$ as a function of the monomer unit number i , for selected energies in the HOMO-LUMO gap. (b) Damping factor β_{MDOS} for the wire of (a), from least-squares fitting of $i = 2, 3, 4$ (dashed line), and of $i = 6, 7, 8$ (dotted line).

least-squares fit to $\ln(\text{MDOS})$ for $i = 2$ to 4 and $i = 6$ to 8 , respectively. Both these curves agree reasonably well with $|\kappa|$, corroborating the picture of metal-induced gap states. We interpret the asymmetry between the left and right parts of MDOS in Fig. 11(a) and (b) as differences on the atomic interfacial contact after optimisation. For example, the erroneous divergence of $\beta_{\text{MDOS}}/2$ around E_F emerges at different energies in Fig. 11(b) for gap states arising from the lower and the upper electrode, with the former seeing the large DOS from the upper electrode, and the latter seeing the large DOS from the lower electrode (see Fig. 7 for comparison).

We briefly comment on the correspondence between the inverse decay length obtained from the molecular density of states and the transport calculations. It is evident that the exponential decay of wavefunctions across the molecular bridge as quantified by the complex-band structure governs both β_{MDOS} and β . However, the spectral properties are determined by the diagonal Green function G_{ii} . Transport is ultimately related to the propagator G_{ij} between unit cells, i.e. $i \neq j$. As suggested

by the above results and the analytic properties of simple π -orbital models the convergence of the latter to the long oligomer limit is much faster, enabling an analysis of the tunnelling regime via the complex k .

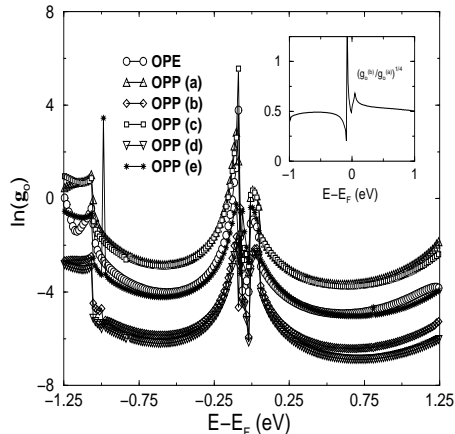


FIG. 12: Logarithm of contact conductance g_o versus energy for all oligomer junctions under study.

C. Contact Conductance

The results of the previous Section elucidate that the inverse decay length β of the conductance in the tunnelling regime is an intrinsic property of the oligomer embedded in the nanojunction. By contrast the prefactor g_o of Eq. 1 is largely determined by the realised interfacial contact. To investigate the so-called contact conductance, in Fig. 12 we present its logarithm versus energy. The curve denoted as OPE corresponds to the contact conductance of similar (or longer) molecular junctions to that of Fig. 1. Those curves indicated by OPP refer to the molecular wires drawn in Fig. 2. All data are obtained after ensuring that the exponential decay of Eq. 1 is fulfilled as explained in Sec. III B. Apparently, g_o depends on the exact atomic contact (whether phenyl or ethynyl group to graphene) as well as the orientation of the phenyl rings with respect to the graphitic ribbons.

It is possible to identify pairs of similar contact conductances from Fig. 12: i) OPE with OPP (e), ii) OPP (a) with OPP (c), and iii) OPP (b) with OPP (d). Although the origin of the first pair is probably fortuitous, pairs ii) and iii) are expected from simple arguments. Moreover, the smaller coupling of the ethynyl-group with respect to the phenyl rings should give rise to the observed reduced g_o of OPE compared to that of planar OPP. The different magnitude of g_o between non-planar oligo-para-phenylene for odd, OPP (c), and even, OPP (e), number of unit cells in the wire, expresses the importance of the length parity in experiments. This is in agreement with our previous discussion. The increased resistance for non-planar alignments of the phenyl end-rings with respect to

the electrodes, e.g., OPP (b), OPP (d) and OPP (e), may be explained as a break-up of the conjugation.

In addition, we estimate the contact conductance ratio between the parallel aligned and twisted phenyl end-ring geometries. We assume, as previously, only π -electrons in an orthogonal basis set. This simple model yields $g_o(E) = \Gamma_L^2 \Gamma_U^2 f(E)$, where, $\Gamma_{L/U}$ corresponds to Hamiltonian matrix elements between the apex carbon atoms located at the wire and the graphene edges. Furthermore, we may write $(g_o^{(b)}/g_o^{(a)})^{1/4} \approx \Gamma^{45^\circ}/\Gamma^{0^\circ}$, which yields $\cos(45^\circ) \approx 0.7$. Considering the oversimplification, this agrees well with the accumulated data (inset of Fig. 12), which give a value around 0.5, apart from the region where the local DOS on the metal side is singular.

Finally, we note the non-trivial energy dependence of the contact conductance, which may hinder simple estimations based on the knowledge of β as those suggested in Ref. [30]. In all our studied cases the contact conductance follows roughly the behaviour of the local DOS at the electrode atomic contacts, with a pronounced peak around the Fermi energy, underlining the importance of the electronic structure of the electrodes. This follows from $f(E)$ being formally decomposed to $\nu_L(E)\nu_U(E)X_M(E)$ in the aforementioned simple model, i.e., being proportional to the product of the metal local DOS, $\nu_L(E)\nu_U(E)$ and a molecular factor $X_M(E)$, which allows for resonant tunnelling at molecular orbital energies. Although $f(E)$ may be a slowly varying function of energy for leads with a seamless local DOS, especially deep in the tunnelling regime, it is not a priori clear that the off-resonant contact conductance is energy independent and can be determined from the on-resonance value [30]. The latter would imply equal contact conductances for perfectly symmetric structures based on OPP (a) and OPP (b) of Fig. 2 although these are at least an order of magnitude different ($\sim 0.5^{-4}$). Clearly, more detailed investigations in diverse molecular junctions are necessary.

V. CONCLUDING REMARKS

We studied the generic properties of off-resonant electron transport across molecular junctions of current experimental interest, formed from oligomers bridging graphitic electrodes. To this end, we used a comprehensive analysis of the electronic structure of the various components in a variety of possible configurations. We showed how the conductance magnitude is crucially determined by the electrode spectral properties, and the exact topological and chemical realisation of the interfacial contact. Most importantly, as a function of the molecular length the tunnelling conductance is almost always an exponentially decreasing function with the inverse decay length given intrinsically by the complex-band structure of the corresponding idealised polymer chain. The properties and accuracy of the latter can be studied independently (cf [76]). Once the Fermi energy is also located with confidence, the damping factor is the-

oretically extracted. This fact has great implications on comparing theoretical and experimental results. A current issue is the discrepancy between those. However, the exact contact geometry, which may have dramatic influence, is largely unknown. Therefore, direct comparison of decay constants in well defined geometries, e.g., in self-assembled monolayers, may shed more light in our understanding of electron transport across molecular junctions.

Acknowledgements

The authors appreciate the kind permission of Marcus Elstner of the TB-DFT team to use his version of

the code. AK would like to thank the *Alexander von Humboldt Stiftung*. Great part of this work has been completed while GF was at Universität Regensburg and supported by the *Graduiertenkolleg Nichtlinearität und Nichtgleichgewicht in Kondensierter Materie*. GF acknowledges current funding by the ATOM CAD project within the *Sixth Framework Programme* of EU.

References

- [1] C. Joachim, J.K. Gimzewski, and A. Aviram, *Nature* **408**, 541 (2000)
- [2] A. Nitzan and M.A. Ratner, *Science* **300**, 1383 (2003)
- [3] T. Seideman, *J. Phys.: Condens. Matter* **15**, R521 (2003)
- [4] A. Aviram and M.A. Ratner, *Chem. Phys. Lett.* **29**, 277 (1974)
- [5] M.A. Reed, C. Zhou, C.J. Muller *et al* *Science* **278**, 252 (1997)
- [6] W. Tian, S. Datta, S. Hong *et al*, *J. Chem. Phys.* **109**, 2874 (1998)
- [7] X.D. Cui, A. Primak, X. Zarate *et al*, *Science* **294**, 571 (2001)
- [8] R.H.M. Smit, Y. Noat, C. Untiedt *et al*, *Nature* **419**, 906 (2002)
- [9] J. Reichert, D. Beckmann, H.B. Weber *et al*, *Appl. Phys. Lett.* **82**, 4137 (2003)
- [10] S. Kubatkin, A. Danilov, M. Hjort *et al*, *Nature* **425**, 698 (2003)
- [11] J.G. Kushmerick, J. Naciri, J. C. Yang, and R. Shashidhar, *Nano Lett.* **3**, 897 (2003)
- [12] L. Patrone, S. Palacin, J. Charlier *et al*, *Phys. Rev. Lett.* **91**, 096802 (2003)
- [13] H. Sakaguchi, A. Hirai, F. Iwata *et al*, *Appl. Phys. Lett.* **79**, 3708 (2001)
- [14] X.D. Cui, A. Primak, X. Zarate *et al*, *J. Phys. Chem. B* **106**, 8609 (2002)
- [15] W. Wang, T. Lee, and M.A. Reed, *Phys. Rev. B* **68**, 035416 (2003)
- [16] B. Xu and N.J. Tao, *Science* **301**, 1221 (2003)
- [17] D.J. Wold and C.D. Frisbie, *J. Am. Chem. Soc.* **123**, 5549 (2001); D.J. Wold, R. Haag, M.A. Rampi *et al*, *J. Phys. Chem. B* **106**, 2813 (2002)
- [18] F. Anariba and R.L. McCreery, *J. Phys. Chem. B* **106**, 10355 (2002)
- [19] T. Ishida, W. Mizutani, Y. Aya *et al*, *J. Phys. Chem. B* **106**, 5886 (2002)
- [20] N.D. Lang and Ph. Avouris, *Phys. Rev. B* **64**, 125323 (2001)
- [21] A. Nitzan, M. Galperin, G-L. Ingold, and H. Grabert, *J. Chem. Phys.* **117**, 10837 (2002)
- [22] Y. Luo, C-K. Wang, and Y. Fu, *J. Chem. Phys.* **117**, 10283 (2002)
- [23] H. Chen, J.Q. Lu, J. Wu *et al*, *Phys. Rev. B* **67**, 113408 (2003)
- [24] Y. Xue and M.A. Ratner, *Phys. Rev. B* **68**, 115406 (2003); *ibid*, **68**, 115407 (2003)
- [25] K. Stokbro, J. Taylor, M. Brandbyge *et al*, *Comp. Mat. Sci.* **28**, 151 (2003)
- [26] V. Mujica, A. Nitzan, S. Datta *et al*, *J. Phys. Chem.* **107**, 91 (2003)
- [27] M.P. Samanta, W. Tian, S. Datta *et al*, *Phys. Rev. B* **53**, R7626 (1996)
- [28] M. Nolan, J.A. Larsson, and J.C. Greer, *Comp. Mat. Sci.* **27**, 166 (2003)
- [29] C.C. Kaun, B. Larade, and H. Guo, *Phys. Rev. B* **67**, 121411 (2003); C.C. Kaun and H. Guo, *Nano Lett.* **3**, 1521 (2003)
- [30] J.K. Tomfohr and O.F. Sankey, *J. Chem. Phys.* **120**, 1542 (2004)
- [31] M. Di Ventra, S.T. Pantelides, and N.D. Lang, *Phys. Rev. Lett.* **84**, 979 (2000)
- [32] P.E. Kornilovitch and A.M. Bratkovsky, *Phys. Rev. B* **64**, 195413 (2001)
- [33] G. Fagas, G. Cuniberti, and K. Richter, *Phys. Rev. B* **63**, 045416 (2001)
- [34] G. Cuniberti, G. Fagas, and K. Richter, *Chem. Phys.* **281**, 465 (2002)
- [35] J. M. Seminario, P. A. Derosa, and J. L. Bastos, *J. Am. Chem. Soc.* **124**, 10266 (2002)
- [36] R. Gutierrez, G. Fagas, K. Richter *et al*, *Europhys. Lett.* **62**, 90 (2003)
- [37] E.G. Emberly and G. Kirczenow, *Phys. Rev. Lett.* **91**, 188301 (2003)
- [38] M.H. Hettler, W. Wenzel W, M.R. Wegewijs *et al*, *Phys. Rev. Lett.* **90**, 076805 (2003)
- [39] T. Tada and K. Yoshizawa, *J. Phys. Chem. B* **107** 8789 (2003)
- [40] R. Gutierrez, F. Grossmann, and R. Schmidt, *ChemPhysChem* **4**, 1252 (2003)
- [41] V. Mujica, M. Kemp, and M.A. Ratner, *J. Chem. Phys.* **101** 6856 (1994)
- [42] A. Onipko, Y. Klymenko, L. Malysheva, and S. Stafström, *Solid State Comm.* **108**, 555 (1998)
- [43] M. Magoga and C. Joachim, *Phys. Rev. B* **57**, 1820 (1998)
- [44] C. Joachim and J.F. Vinuesa, *Europhys. Lett.* **33**, 635

- (1996)
- [45] M. Magoga and C. Joachim, Phys. Rev. B **56**, 4722 (1997)
- [46] H.M. McConnell, J. Chem. Phys. **35**, 508 (1961)
- [47] J.W. Evenson and M. Karplus, J. Chem. Phys. **96**, 5272 (1992)
- [48] J.R. Reimers and N.S. Hush, J. Photochem. Photobiol. A **82**, 31 (1994)
- [49] A. Nitzan, J. Phys. Chem. A **105**, 2677 (2001)
- [50] E. Gudowska-Nowak, G. Papp, and J. Brickmann, Chem. Phys. **232**, 247 (1998)
- [51] A. Lahmidi and C. Joachim, Chem. Phys. Lett. **381**, 381 (2003)
- [52] C. Joachim and M. Magoga, Chem. Phys. **281** 347 (2002)
- [53] J.K. Tomfohr and O.F. Sankey, Phys. Rev. B **65**, 245105 (2002)
- [54] W. Kohn, Phys. Rev. **115**, 809 (1959)
- [55] V. Heine, Proc. Phys. Soc. **81**, 300 (1963)
- [56] S. Datta, *Electronic Transport in Mesoscopic Systems*, Cambridge University Press, Cambridge (1995)
- [57] A. Nitzan, Annu. Rev. Phys. Chem. **52**, 681 (2001)
- [58] G. Fagas, A. Kambili, and M. Elstner, to be published in Chem. Phys. Lett., cond-mat/0308114
- [59] F. Barra and P. Gaspard, J. Phys. A: Math. Gen. **32**, 3357 (1999)
- [60] C.D. Simpson, J.D. Brand, A.J. Berresheim *et al*, Chem.-Eur. J. **8**, 1424 (2002)
- [61] M. Fujita, K. Wakabayashi, K. Nakada, and K. Kusakabe, J. Phys. Soc. Japan **65**, 1920 (1996)
- [62] K. Nakada, M. Fujita, G. Dresselhaus, and M.S. Dresselhaus, Phys. Rev. B **54**, 17954 (1996)
- [63] Y. Miyamoto, K. Nakada, and M. Fujita, Phys. Rev. B **59**, 9858 (1999)
- [64] T. Kawai, Y. Miyamoto, O. Sugino, and Y. Koga, Phys. Rev. B **62**, R16349 (2000)
- [65] F.L. Shyu, M.F. Lin, C.P. Chang *et al*, J. Phys. Soc. Japan **70**, 3348 (2001)
- [66] G. Fagas, R. Gutierrez, K. Richter *et al*, to be published in Macromol. Symp.
- [67] T. Frauenheim, G. Seifert, M. Elstner *et al*, Phys. Stat. Sol. (b) **217**, 41 (2000)
- [68] M. Elstner, D. Porezag, G. Jungnickel *et al*, Phys. Rev. B **58**, 7260 (1998)
- [69] A. Pecchia, M. Gheorghe, A. Di Carlo, and P. Lugli, Synth. Met. **138**, 89 (2003)
- [70] M. Elstner, T. Frauenheim, and S. Suhai, to be published in J. Mol. Struct. (THEOCHEM)
- [71] S. Sanvito, C.J. Lambert, J.H. Jefferson, and A.M. Bratkovsky, Phys. Rev. B **59**, 11936 (1999)
- [72] D.H. Lee and J.D. Joannopoulos, Phys. Rev. B **23**, 4988 (1981)
- [73] C. Ambrosch-Draxl, J.A. Majewski, P. Vogl, and G. Leising, Phys. Rev. B **51**, 9668 (1995)
- [74] S. Guha, W. Graupner, R. Resel *et al*, J. Phys. Chem. A **105**, 6203 (2001)
- [75] U. Landman, R.N. Barnett, A.G. Schebakov *et al*, Phys. Rev. Lett. **85** (2000) 1958
- [76] S. Piccinin, A. Selloni, S. Scandolo *et al*, J. Chem. Phys. **119**, 6729 (2003)
- [77] F. Picaud, A. Smogunov, A. Dal Corso *et al*, J. Phys.: Condens. Matter **15**, 3731 (2003)